Supporting Information

Iron Pyrite Nanocrystal Inks: Solvothermal Synthesis, Digestive Ripening, and Reaction Mechanism

Tara S. Yoder[†], Jacqueline E. Cloud[†], G. Jeremy Leong[†], Doreen F. Molk[†], Matthew Tussing[†], Jonathan Miorelli[†], Chilan Ngo[‡], Suneel Kodambaka[‡], Mark E. Eberhart[†], Ryan M. Richards[†], and Yongan Yang*[,†]

† Department of Chemistry and Geochemistry, Colorado School of Mines, Golden, Colorado 80401

‡ Department of Materials Science and Engineering, University of California Los Angeles, Los Angeles, California 90095

Synthetic Conditions

Four solvents were studied in the course of exploring the most effective one for synthesizing FeS_2 nanocrystal (NC) inks. When using water as the solvent, we adapted a method reported in the literature and studied the ligand effect.[1] First, 0.2 mmol of iron diethyldithiocarbamate (FeE_3,100 mg), 2 mmol of ligand, and 4 mL of water were added into a Teflon-lined stainless steel autoclave vessel (Parr Instr., model 4749, 23 mL). Then, the reactor was sealed and autoclaved at 180 ^oC in a preheated muffle furnace for 18 h. After cooling the reactor to room temperature in air, the solvent and the dark-grey product were separated via centrifugation at a relative centrifugal force (RCF) of 1228 G (3100 rpm on a RCF-fixed Medilite centrifuge) for five minutes. The collected solid was further washed with a mixture of chloroform and carbon disulfide for several times, until the centrifuged supernatant was clear and colorless. The obtained nanoparticles were not soluble in the solvents we tested, such as chloroform, toluene, hexane, or ethanol.

Three organic solvents tested were octadecylamine (ODA), toluene, and dimethylformamide (DMF). When using organic chemicals as the solvents, extra sulfur was necessary to produce phase-pure FeS_2 NCs. For example, in the case of using toluene as the solvent, FeE_3 (100 mg), sulfur (64 mg – FeE_3:S ratio of 1:10, denoted as 10S), and solvent (4 mL) were added into an autoclave vessel. When the effects of ligand identity and concentration were explored, a sufficient amount of ODA was also added to result in a 0.1M – 0.5M solution. Then, the reactor was sealed and autoclaved at 180 - 240 °C for 18 h in a preheated muffle furnace. To study the effect of stirring, the reactor was put in a sand bath, and the stir plate was set at 700 rpm.

Solvent Screening

ODA (SI-Figure 1) – In ODA, XRD data confirm (**SI-Figure 1A**) that nanocrystalline FeS_2 was obtained in the temperature range of 190 - 240 °C. At 180 °C, some unknown impurities were also present. However, the problem remained that the obtained NCs were not soluble in any of the solvents we tested, due to the considerable amount of aggregates as shown in the TEM image (**SI-Figure 1B**). In addition, the unreacted ODA was very difficult to remove, due to its solid state at room temperature and interaction with the ligands on the FeS_2 NC surfaces. Thus, ODA only was used as the passivating ligand in the following studies.

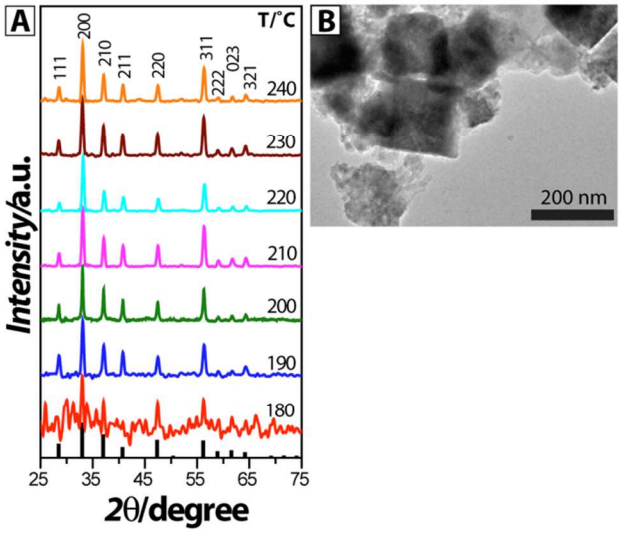

SI-Figure 1. Studies of the products obtained in ODA. (A) XRD data for the products synthesized at various temperatures of 180 – 240 °C, by using FeE_3 + 10S and reaction duration of 18 h. (B) TEM image of the product obtained at 200 °C. Black stick pattern is for the FeS_2 standard (JCPDS No. 01-071-0053).

Toluene (SI-Figure 2) – Toluene was selected as a solvent due to its capability for dissolving ODA and FeE_3. **SI-Figure 2A** shows the XRD data of the obtained FeS_2 NCs at temperatures between 180 and 240 °C. Unknown impurities were present in XRD profiles, as labelled with circles in **SI-Figure 2A**. To understand the origin of this phenomenon, three control experiments were conducted (**SI-Figure 2B**): FeE_3 + 10S (pink), FeE_3 only (cyan), and sulfur only (brown). In addition to the contaminant peaks in **SI-Figure 2A**, several new unknown peaks (squares) can be observed. The control study indicated that the impurities were either associated with sulfur-containing chemicals (circles, **SI-Figure 2A-i**) or side products due to deficient temperatures, matching the major peaks from **SI-Figure 2A-ii** (squares). The fact that pyrite was not produced in the absence of sulfur indicated that sulfur played a critical role in producing phase-pure FeS_2 in toluene. Furthermore, while the purification process became easier compared to using ODA as the solvent, the products were still insoluble. Thus, toluene was not a suitable option.

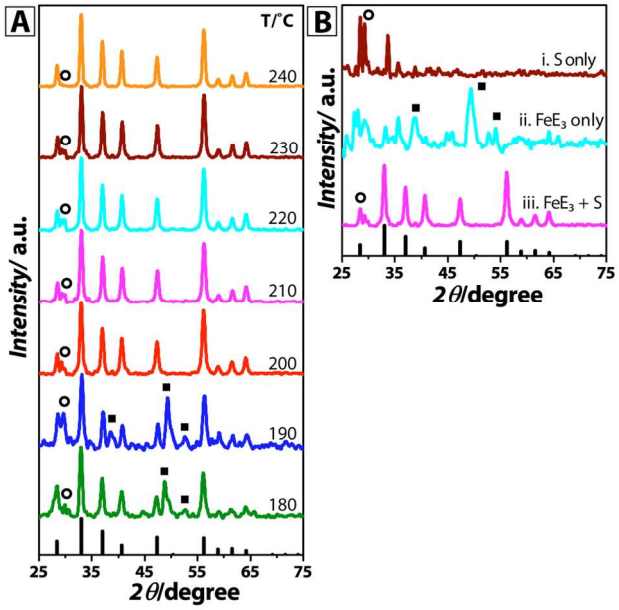

SI-Figure 2. XRD studies of the products obtained in toluene. (A) XRD spectra obtained from samples produced at various temperatures between 180 and 240 °C by using FeE_3 + 10 S for 18 h. (B) Shorter time durations of 2 h (red), 4 h (blue), and 6 h (green) at 200 °C. (C) Three control reactions using FeE_3 + 10S (pink), FeE_3 only (cyan), and S only (brown) at 200 °C for 18 h. Black stick pattern is for the FeS_2 standard (JCPDS No. 01-071-0053); squares and circles denote the unknown impurities.

DMF (SI-Figure 3) – DMF was chosen as the new solvent, due to its capability of dissolving both ODA and FeE_3. The XRD data in **SI-Figure 3A** showed that the best temperatures were 180 °C and 190 °C. At the higher temperatures of 200 – 240 °C, surprisingly, mixtures of iron pyrite (bottom sticks and stars) and pyrrhotite Fe_xS_y (top sticks and squares) were obtained. Learning from ODA and toluene, control reactions were also studied using only DMF without ODA. Solid product was not obtained when using only S (**SI-Figure 3B-i**). In the case of FeE_3 only (without extra S), some unknown impurities other than FeS_2 were produced (**SI-Figure 3B-ii**). After adding extra sulfur (10S), phase-pure FeS_2 was obtained (**SI-Figure 3B-iii**).

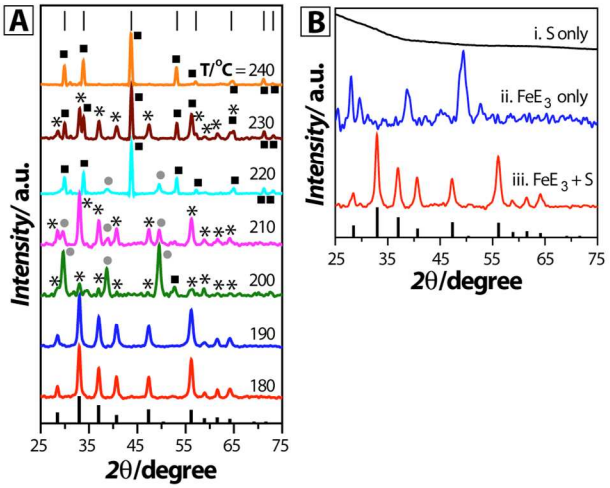

SI-Figure 3. XRD spectra of the products obtained in DMF. (A) XRD data obtained from samples produced at various temperatures between 180 and 240 °C, by using FeE_3 + 10 S for 18 h. (B) Three control reactions using FeE_3 + 10 S (red), FeE_3 only (blue), and S only (black) at 190 °C for 18 h. Black stick pattern is for the FeS_2 standard (JCPDS No. 01-071-0053), the squares and top lines identify pyrrhotite, and the circles denote an unmatched impurity.

Lower ODA Concentration with Stirring (SI-Figure 4)

When a lower concentration of 0.1M ODA was combined with stirring, the increased mass transport significantly improved the dispersity of FeS_2 NCs. Many aggregates were present (**SI-Figure 4A**) in addition to a large amount of free particles (**SI-Figure 4B**).

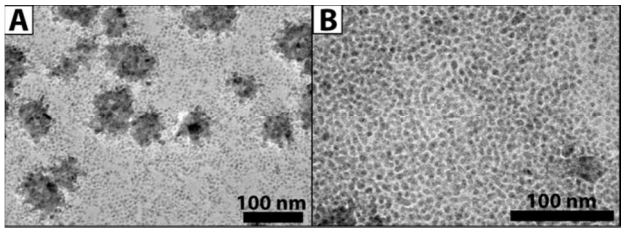

SI-Figure 4. TEM images of the product obtained by using 0.1M ODA in DMF with stirring at 190 °C for 22 h. (A) Panoramic view of both individual particles and aggregates, and (B) close-up of only individual particles.

The Effect of Ligands in DMF on Synthesis of FeS_2 (SI-Figure 5)

Four additional organic ligands – ODX, DDA, OLA, and TOPO – were assessed with the stirred reaction system under the same reaction conditions as ODA. Only the TOPO system produced phase-pure FeS_2, as shown by the XRD data in **SI-Figure 5A**. However, the TEM images reveal that the TOPO did not effectively passivate the particles, resulting in insoluble aggregates (**SI-Figure 5B**).

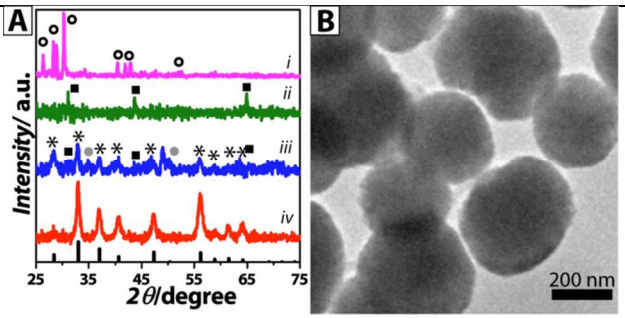

SI-Figure 5. (A) XRD data of the obtained products when using DMF solutions with 0.5M ODX (*i*), DDA (*ii*), OLA (*iii*), and TOPO (*iv*). All reactions were stirred, using FeE_3, 6S, at 190 °C for 22 h. Black stick pattern and stars are for the FeS_2 standard (JCPDS No. 01-071-0053). The squares and dots denote impurities that could not be matched by any of the XRD patterns in the database or any known iron sulfide standards. (B) TEM image of the product when TOPO was used (A-iv), showing only aggregates without any individual NCs.

Additional Study of the Surface Effect on Far-IR Spectra (SI-Figure 6)

Far-IR spectra of the TOPO-passivated (red) and ligand-free (blue) FeS_2 NCs show positive absorption peaks for the former sample and negative peaks for the latter.

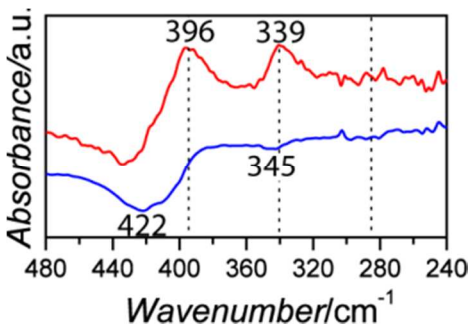

SI-Figure 6. Far-IR spectra of TOPO-passivated FeS_2 NCs (red) and ligand-free FeS_2 NCs (blue).

The Development of Synthetic Conditions for Digestive Ripening (SI-Figures 7 and 8)

Our initial study of digestive ripening explored the use of four ligands (ODA, OLA, DDA, and DDT (dodecanethiol)) in toluene, by using purified FeS_2 NCs from the solvothermal synthesis. The ligands and solvent were chosen based on previous literature methods;[2-4] ODA was also the ligand used in our solvothermal synthesis. The ligand concentration was 0.75 M and the refluxation duration was 24 ± 1 h. As shown by the TEM images in **SI-Figure 7**, all systems produced seriously aggregated products. Nevertheless, the DDA system also showed a small number of individual particles, implying the promise of this system. We hypothesized that the unsuccessful results were due to the instability of the purified FeS_2 NCs in toluene and the lack of excess sulfur.

Thus, subsequently, we used DMF (the original solvent during the solvothermal reaction) instead of toluene as the solvent, changed the starting material to the unpurified FeS_2 solution directly out of the solvothermal reaction, and added six portions of sulfur versus FeS_2. Surprisingly, the use of ODA resulted in a poorer morphology (**SI-Figure 8A**). In contrast, the DDA system produced high-quality

colloidal FeS_2 NCs, as shown in **Figure 5** in the main text, while the product without using excess sulfur was obviously inferior (**SI-Figure 8B**).

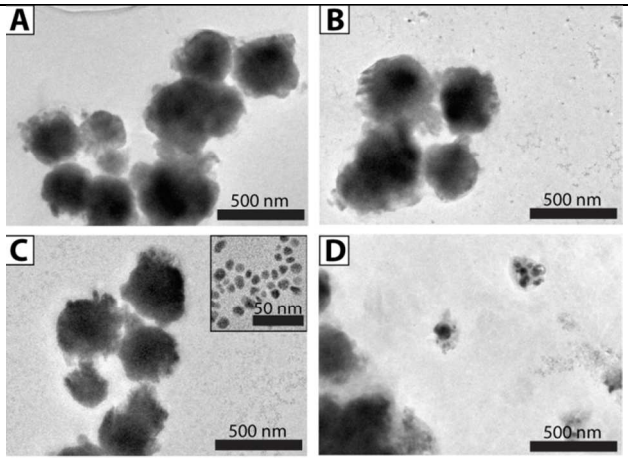

SI-Figure 7. TEM images of the digestively ripened products using purified FeS_2 NCs as the starting material, toluene as the solvent, and different chemicals as the ligand: (A) ODA, (B) OLA, (C) DDA, and (D) DDT. The inset in (C) shows some individual particles formed.

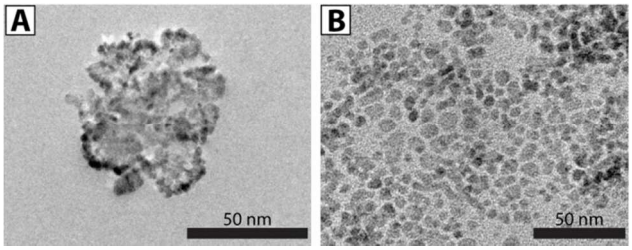

SI-Figure 8. (A) TEM image of the obtained product after digestive ripening of the unpurified FeS_2 solution from the solvothermal reaction, using *ODA* as the ligand, DMF as the solvent, and *excess sulfur (6S)*. (B) TEM image of the obtained product after digestive ripening of the unpurified FeS_2 solution from the solvothermal reaction, using *DDA* as the ligand, DMF as the solvent, and *no excess sulfur*.

Additional TEM Images of the Digestive Ripening Product (**SI-Figure 9**)

In addition to **Figure 5A** in the main text, additional TEM images of two sets of larger areas on the grid are shown in **SI-Figure 9** to demonstrate the high quality of the digestive ripening product. While occasionally some areas show slight aggregations, monolayers of well-ordered NCs can be observed on nearly the whole grid, for instance, two exemplary areas in **SI-Figures 9C** and **F**. The narrow size distribution of the obtained NCs can be embodied by the histogram of 600 particles (**SI-Figures 9G**), showing an average size of 5.8 ± 0.8 nm in diameter.

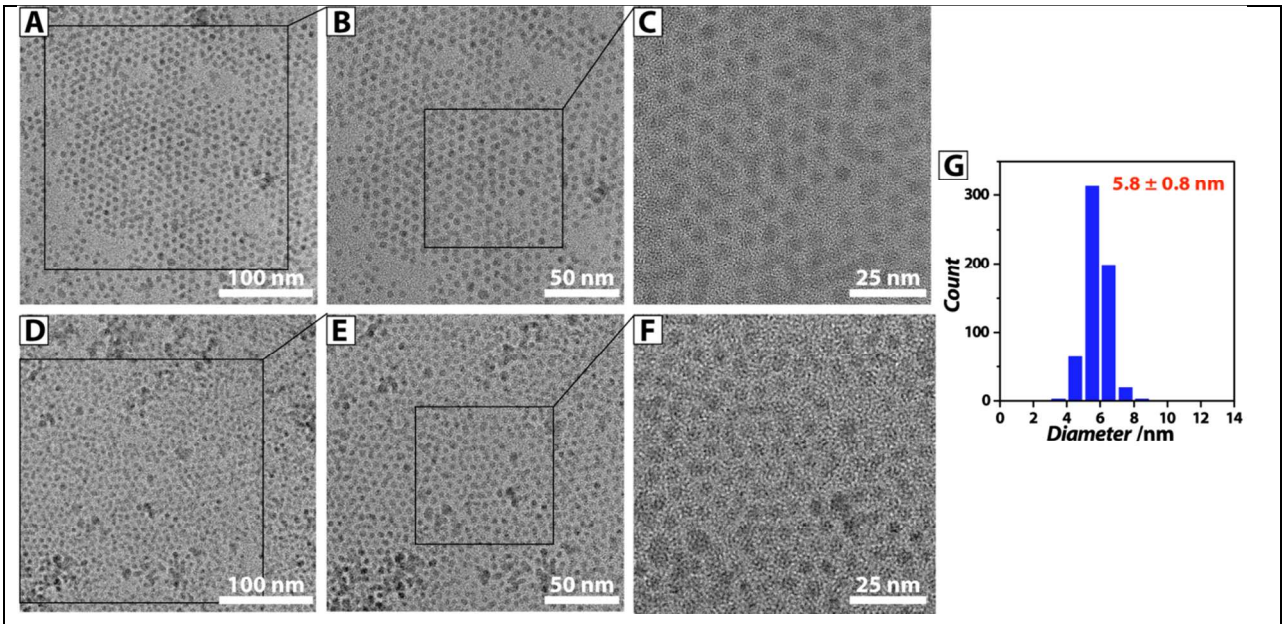

SI-Figure 9. TEM images of the digestively ripened FeS_2 NCs in different areas on the TEM grid (A-C and D-F) and the corresponding histogram of the size distribution for 600 particles (G).

Computational Details (SI-Figure 10)

The presence of a chemical bond necessitates that there exists a ridge of charge density connecting the bound atoms as well as a saddle point, known as the bond critical point (bond CP), which sits at the local minimum along the ridge (**Figure 6**). A good deal of information about the nature of a bond can be inferred by the character of the density at the bond critical point as changes to the amount of charge (ρ) at a bond CP and shape of the density near the bond CP correspond to changes to the bond itself.[5] The shape of the charge density near a given point can be well approximated by the Hessian,[6, 7] which has the same transformation properties of a second degree polynomial known as the representation quadric. For a bond CP the representation quadric defines a hyperboloid of two sheets, which can be parameterized by its exterior angles defined here as 2θ and 2φ, respectively (see **SI-Figure 10**). What is important is that these angles describe the directions along which the curvature of the charge density goes to zero and therefore small values of θ and φ correspond to a flat charge density near the bond CP, while larger values of θ and φ correspond to a more pronounced ridge within the charge density. An appropriate metric that incorporates both the amount of charge as well as the shape of the density was developed by Knoerr and Eberhart,[8] who showed that the amount of charge that must be lost from a bond CP in order to "break" the bond can be approximated using:

$$\rho \sin^2(\theta) \quad \text{and} \quad \rho \sin^2(\varphi) \qquad (1)$$

Observed changes to calculated values for equation 1 serves as an appropriate metric for observing changes to specific bonds. Calculated values at specified bond CPs of $\rho \sin^2(\theta)$ for the non-protonated ligand, as well as protonation at a carbon and sulfur are given in **SI-Table 1**.

When studying protonation and nucleophilic attack, geometry optimizations were used. Geometry optimization calculations, where a nucleophile (HO^- or SH^-) is placed near the protonated carbon (within an angstrom or two), resulted in bond formation between the nucleophile and the protonated carbon. Attack from both nucleophiles resulted in the loss of a C-S bond causing the ligand to partially break away from the central Fe atom and leaving behind a free S atom attached to the Fe.

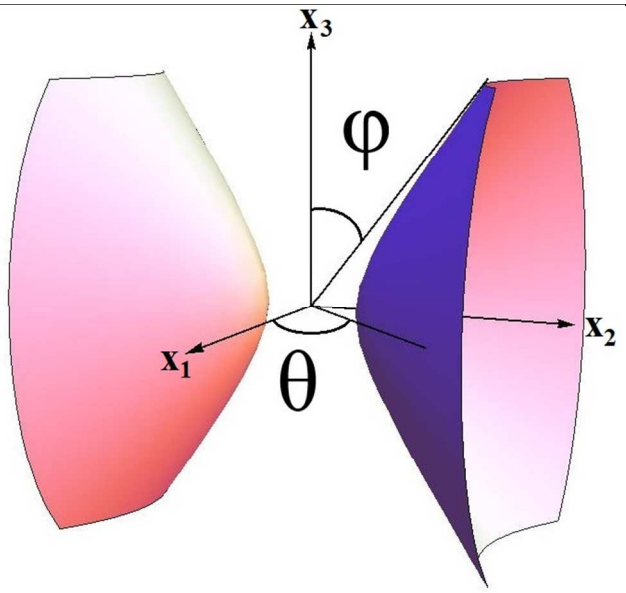

SI-Figure 10. A graphical depiction of a hyperboloid of two sheets, with the geometry of the hyperboloid described by the angles θ and φ. The axes x_1, x_2, and x_3 are the directions along the gradient of the density goes to zero, in this case x_2 lies along the bond path. The angles describe the direction from the bond CP along which the curvature goes to zero, thus smaller values of θ and φ indicate a more flat density near the bond CP and as such acts as a measure of the amount of density shared between atoms. See literature for further detail.[6-8]

SI-Table 1. Properties of the charge density at the indicated bond critical points.

Protonation Site	**Bond CP**	**ρ [e^- Bohr^{-3}]**		**ρ $\sin^2(\theta)$**		**ρ $\sin^2(\varphi)$**	
		LDA	PBE	LDA	PBE	LDA	PBE
None	Fe-S	0.0631	0.055	0.0499	0.0440	0.0491	0.0434
	S-C	0.213	0.207	0.0938	0.0922	0.0872	0.0850
Carbon	S'-CH	0.150	0.138	0.0880	0.0839	0.0855	0.0815
	S"-CH	0.177	0.174	0.0936	0.0922	0.0908	0.0894
Sulfur	Fe-S'H	0.0231	N/A	0.0197	N/A	0.0194	N/A
	C-S'H	0.204	0.201	0.0978	0.0974	0.0882	0.0861

The reported results were computed using a TZ2P basis set[9] and local density approximation (LDA) exchange/correlation potential.[10] Results were also confirmed using the generalized gradient approximation exchange and correlation functional developed by Perdew, Burke, and Ernzerhof (PBE).[11] Note: At the PBE level of calculation no Fe-S'H bond CP could be recovered, hence why there is no data provided for that bond CP.

References:

(1) Chen, X. Y.; Wang, Z. H.; Wang, X.; Wan, J. X.; Liu, J. W.; Qian, Y. T., *Inorg. Chem.* **2005,** *44*, 951-954.

(2) Prasad, B. L. V.; Stoeva, S. I.; Sorensen, C. M.; Klabunde, K. J., *Langmuir* **2002,** *18*, 7515-7520.

(3) Prasad, B. L. V.; Stoeva, S. I.; Sorensen, C. M.; Klabunde, K. J., *Chem. Mater.* **2003,** *15*, 935-942.
(4) Lin, X. M.; Sorensen, C. M.; Klabunde, K. J., *J. Nanopart. Res.* **2000,** *2*, 157-164.
(5) *The Quantum Theory of Atoms in Molecules: From Solid State to DNA and Drug Design*. Wiley-VCH: 2007.
(6) Eberhart, M. E., *Acta Mater.* **1996,** *44*, 2495 - 2504.
(7) Eberhart, M. E.; Jones, T. E., *Phys. Rev. B* **2012,** *86*, 134106.
(8) Knoerr, E. H.; Eberhart, M. E., *J. Phys. Chem. A* **2001,** *105*, 880-884.
(9) Van Lenthe, E.; Baerends, E. J., *J. Comput. Chem.* **2003,** *24*, 1142-1156.
(10) Vosko, S. H.; Wilk, L.; Nusair, M., *Can. J. Phys.* **1980,** *58*, 1200-1211.
(11) Perdew, J. P.; Burke, K.; Ernzerhof, M., *Phys. Rev. Lett.* **1996,** *77*, 3865-3868.